



Phonon-mediated dimensional crossover in bilayer CrI₃M. Rodriguez-Vega ^{1,2,*}, Ze-Xun Lin,^{1,2,*} A. Leonardo ^{3,4}, A. Ernst,^{5,6} G. Chaudhary,⁷
M. G. Vergniory,^{3,8} and Gregory A. Fiete^{2,1,9}¹Department of Physics, The University of Texas at Austin, Austin, Texas 78712, USA²Department of Physics, Northeastern University, Boston, Massachusetts 02115, USA³Donostia International Physics Center, Paseo Manuel de Lardizabal 4, 20018 San Sebastian, Spain⁴Applied Physics Department II, University of the Basque Country UPV/EHU, Bilbao, Spain⁵Institut für Theoretische Physik, Johannes Kepler Universität, A 4040 Linz, Austria⁶Max-Planck-Institut für Mikrostrukturphysik, Weinberg 2, D-06120 Halle, Germany⁷James Franck Institute, Department of Physics, The University of Chicago, Chicago, Illinois 60637, USA⁸IKERBASQUE, Basque Foundation for Science, Bilbao, Spain⁹Department of Physics, Massachusetts Institute of Technology, Cambridge, Massachusetts 02139, USA

(Received 30 March 2020; accepted 7 August 2020; published 21 August 2020)

In bilayer CrI₃, experimental and theoretical studies suggest that the magnetic order is closely related to the layer stacking configuration. In this work, we study the effect of dynamical lattice distortions, induced by nonlinear phonon coupling, in the magnetic order of the bilayer system. We use density functional theory to determine the phonon properties and group theory to obtain the allowed phonon-phonon interactions. We find that the bilayer structure possesses low-frequency Raman modes that can be nonlinearly activated upon the coherent photoexcitation of a suitable infrared phonon mode. This transient lattice modification in turn inverts the sign of the interlayer spin interaction for parameters accessible in experiments, indicating a low-frequency light-induced antiferromagnet-to-ferromagnet transition.

DOI: [10.1103/PhysRevB.102.081117](https://doi.org/10.1103/PhysRevB.102.081117)

Introduction. The control of ordered states of matter such as magnetism, superconductivity, or charge- and spin-density waves is one of the more sought after effects in the field. In equilibrium, this can be achieved by turning the knobs provided by temperature, strain, pressure, or chemical composition. However, the nature of these methods limits the possibility to integrate the materials into devices for technological applications due to undesirably slow control and nonreversibility. In recent years, a new approach has emerged which allows *in situ* manipulation: driving systems out of equilibrium by irradiating them with light [1–33]. Recent experiments have demonstrated the existence of Floquet states in topological insulators [34,35], the possibility to transiently enhance superconductivity [36–38], the existence of light-induced anomalous Hall states in graphene [39], light-induced metastable charge-density-wave states in 1T-TaS₂ [40], optical pulse-induced metastable metallic phases hidden in charge ordered insulating phases [41,42], and metastable ferroelectric phases in titanates [43].

Finding suitable platforms to realize nonequilibrium transitions represents the first main challenge. Recently, interest in the van der Waals bulk ferromagnet chromium triiodide (CrI₃) [44,45] has been renewed with the discovery that it is stable in its monolayer form, where the chromium atoms arrange in a hexagonal lattice and the iodine atoms order on a side-sharing octahedral cage around each chromium atom

as shown in Figs. 1(a) and 1(b). Monolayer CrI₃ presents out-of-plane magnetization stabilized by anisotropies [46] and a Curie temperature $T \sim 45$ K [47]. The origin of the anisotropies is still a subject of intense theoretical and experimental investigations [48–50].

In bulk form, CrI₃ exhibits a structural phase transition near $T = 210$ – 220 K. This structural transition is accompanied by an anomaly in the magnetic susceptibility, but no magnetic ordering [45]. At $T = 61$ K, CrI₃ exhibits a transition from paramagnet to ferromagnet [45], with an easy-axis perpendicular to the two-dimensional planes. Evidence suggests that CrI₃ is a Mott insulator with a band gap close to 1.2 eV [44,45]. Recent experiments have measured large tunneling magnetoresistance [51,52], suggesting potential applications in spintronics devices.

Bilayer CrI₃ (b-CrI₃) presents an antiferromagnetic (AFM) ground state [47,52–55], with monoclinic crystal structure [Figs. 1(c) and 1(d)]. Single-spin microscopy [56] and polarization-resolved Raman spectroscopy [57] measurements have established a strong connection between the magnetic order and the stacking configuration in few-layers CrI₃. Furthermore, it has been shown that the magnetic order can be controlled in equilibrium by doping [58] and applying pressure [59] to b-CrI₃. These results have been accompanied by theoretical studies, which find that the AFM order is linked to the lattice configuration [60–63]. In particular, orbital-dependent magnetic force calculations show that the stacking pattern can suppress or enhance the e_g - t_{2g} interaction and correspondingly favor an AFM or ferromagnetic (FM) order [61].

*These two authors contributed equally to this work.

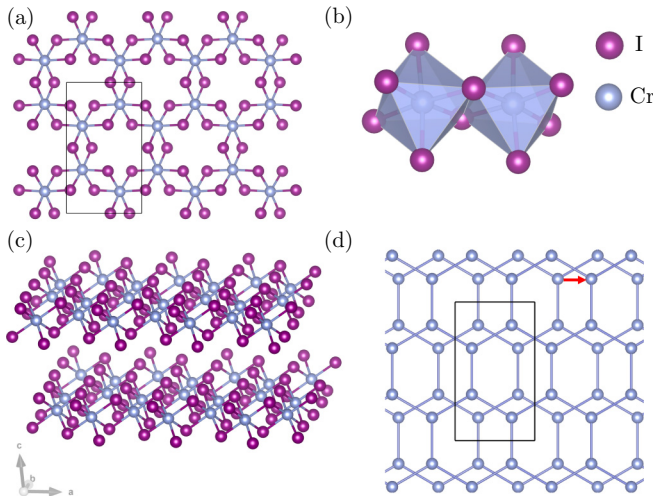


FIG. 1. (a) Monolayer CrI_3 lattice structure. The conventional unit cell is shown with solid lines. (b) Cr^{+3} atoms surrounded by an edge-sharing I octahedral cage. (c) b- CrI_3 crystal structure with space group $C2/m$ associated with the AFM ground state. The top layer is shifted with respect to the bottom layer by $[1/3\ 0\ 0]$. (d) Top view with I atoms suppressed for clarity. The red arrow indicates the relative shift. The black box indicates the conventional unit cell. The lattice structures were created with VESTA [64].

In this Rapid Communication, we leverage these theoretical and experimental results in equilibrium, and consider the possibility to dynamically tune the magnetic order in b- CrI_3 using low-frequency light to coherently drive suitable phonon modes. We start with a group theory analysis to determine the feasibility of the nonlinear phonon process required. Then, we perform first-principles calculations to find phonon frequencies, eigenmodes, and nonlinear phonon coupling strengths. We then analyze the equations of motion for the driven phonons and their impact on the lattice structure. Finally, we determine the effect of such transient lattice deformations on the magnetic order and find the possibility to induce a sign change in the interlayer exchange interaction using experimentally accessible parameters.

Group theory analysis. Recent first-principles studies indicate that there is a direct relation between the magnetic ground state and the relative stacking order between the layers [60,62,65]. The FM phase presents an AB stacking with space group $R\bar{3}$ (point group S_6), while the AFM ground state is accompanied by an AB' stacking with space group $C2/m$ and point group C_{2h} [60] [Fig. 1(d)]. AFM and FM structures are related by a relative shift of the layers leaving each individual layer unaltered. Since experiments find AFM order in the ground state [47], in our analysis we assume the configuration corresponding to the C_{2h} space group. The primitive unit cell contains 4 Cr and 12 I atoms, for a total of $N = 16$ atoms. The conventional to primitive unit cell transformation, and the C_{2h} point group character table are listed in [66]. The total number of phonon modes is then $3N = 48$. We obtain that the equivalence representation is given by $\Gamma^{\text{equiv}} = 5A_g \oplus 3B_g \oplus 3A_u \oplus 5B_u$. In the C_{2h} point group, the representation of the vector is $\Gamma_{\text{vec}} = 2A_u \oplus B_u$, which leads to the lattice vibration representation $\Gamma_{\text{latt.vib.}} = \Gamma^{\text{equiv}} \otimes$

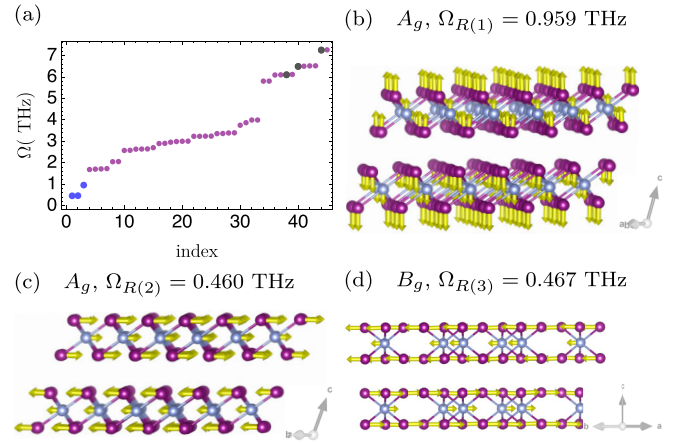


FIG. 2. (a) b- CrI_3 phonon frequencies in the space group $C2/m$ and AFM ground state. The blue dots correspond to Raman modes involving layer relative shifts. The gray dots correspond to IR modes that directly couple to the light pulse. The acoustic modes are not shown. (b)–(d) b- CrI_3 low-frequency Raman phonon displacements relevant for the nonlinear dynamics.

$\Gamma_{\text{vec}} = 13A_g \oplus 11B_g \oplus 11A_u \oplus 13B_u$. From the symmetry of the generating functions (see the Supplemental Material [66]), 24 modes are Raman active (13 with totally symmetric A_g representation and 11 with B_g representation) and 24 infrared active modes [67].

Here, we posit that a Raman mode involving a relative shift between the layers might influence the magnetic order. In order to test if such a mode is allowed by symmetry, we construct the projection operators [68–70] $\hat{P}_{kl}^{(\Gamma_n)} = \frac{l_n}{h} \sum_{C_\alpha} [D_{kl}^{(\Gamma_n)}(C_\alpha)]^* \hat{P}(C_\alpha)$, where Γ_n are the irreducible representations, C_α are the elements of the group, $D_{kl}^{(\Gamma_n)}(C_\alpha)$ is the irreducible matrix representation of element C_α , h is the order of the group, and l_n is the dimension of the irreducible representation. Finally, $\hat{P}(C_\alpha)$ are $3N \times 3N$ matrices that form the displacement representation. Applying the projection operators \hat{P}^{A_g} and \hat{P}^{B_g} to random displacements of the atoms, we find that modes with one layer uniformly displaced in the $[1\ 1\ 0]$ direction, while the other in the $[\bar{1}\ \bar{1}\ 0]$ direction is allowed by symmetry and belong to the totally symmetric A_g representation [Fig. 2(c)]. Similarly, modes where one layer is displaced in the $[0\ 0\ 1]$ direction and the other one in the $[0\ 0\ \bar{1}]$ belongs to the A_g representation [Fig. 2(b)]. On the other hand, layer displacements in the directions $[\bar{1}\ 1\ 0]$ and $[1\ \bar{1}\ 0]$ belong to the B_g representation [Fig. 2(d)]. We will show that these Raman modes can be manipulated via indirect coupling with light to control the magnetic order.

Phonons. Once we determine that relative-shift modes are allowed by symmetry, we calculate the phonon frequencies using density functional perturbation theory and finite difference methods as implemented in QUANTUM ESPRESSO [71,72] and VASP [73,74], respectively. We find excellent agreement among all the approaches considered (see [66] for details).

In Fig. 2(a), we plot the full set of frequencies of the Γ -point phonons. We find that the three low-frequency modes (apart from the three omitted zero-frequency acoustic modes) are Raman active, and correspond to relative displacement

between the layers in different directions, in agreement with the group theory results. The lowest-frequency mode, $\Omega = 0.460$ THz, belongs to the A_g representation, and the real-space displacement is shown in Fig. 2(c). The next phonon mode is very close in frequency, $\Omega = 0.467$ THz; however, it belongs to the B_g representation [Fig. 2(d)]. The mode with frequency $\Omega = 0.959$ THz belongs to the A_g representation and corresponds to a relative displacement perpendicular to the layers, as shown in Fig. 2(b).

Nonlinear phonon processes have been proposed for transient modification of the symmetries of the system, which can be accompanied by changes in the ground-state properties [3,4,7–9,12–15]. Now, we derive the nonlinear phonon potential resulting from coupling between infrared (Q_{IR}) and Raman (Q_{R}) active modes in b-CrI₃. In an invariant polynomial under the operations of a given group, coupling between two modes is allowed only if it contains the totally symmetric representation [68–70]. In principle, an IR mode is allowed to couple nonlinearly to all A_g and B_g Raman modes in the C_{2h} point group. However, as we will show, we can focus on the modes involving relative motion between the layers because they possess very low frequency, compared with the rest of the Raman phonons. Up to cubic order, the nonlinear potential functional including the three low-frequency phonon modes is given by

$$\begin{aligned}
 V[Q_{\text{IR}}, Q_{\text{R}(i)}] &= \frac{1}{2}\Omega_{\text{IR}}^2 Q_{\text{IR}}^2 + \sum_{i=1}^3 \frac{1}{2}\Omega_{\text{R}(i)}^2 Q_{\text{R}(i)}^2 \\
 &+ \sum_{i=1}^2 \frac{\beta_i}{3} Q_{\text{R}(i)}^3 + Q_{\text{IR}}^2 \sum_{i=1}^2 \gamma_i Q_{\text{R}(i)} + \delta Q_{\text{R}(1)}^2 Q_{\text{R}(2)} \\
 &+ \epsilon Q_{\text{R}(1)} Q_{\text{R}(2)}^2 + Q_{\text{R}(3)}^2 \sum_{i=1}^2 \zeta_i Q_{\text{R}(i)}. \quad (1)
 \end{aligned}$$

The numerical value of the coefficients is obtained using first-principles calculations. In the Supplemental Material [66] we outline the procedure we used following Ref. [4], we plot the energy surfaces obtained by varying the corresponding phonon mode amplitudes, and display the numerical values of the coefficients obtained by fitting Eq. (1).

Under an external drive with frequency Ω , the potential acquires the time-dependent term [75,76] $V_D[Q_{\text{IR}}] = \mathbf{Z}^* \cdot \mathbf{E}_0 \sin(\Omega t) F(t) Q_{\text{IR}}$, where \mathbf{E}_0 is the electric field amplitude, and \mathbf{Z}^* is the mode effective charge vector [75,77]. $F(t) = \exp\{-t^2/(2\tau^2)\}$ is the Gaussian laser profile, with variance τ^2 . Assuming that damping can be neglected, the general differential equations governing the dynamics of one infrared mode coupled to m Raman modes are obtained from the relations $\partial_t^2 Q_{\text{R}(i)} = -\partial_{Q_{\text{R}(i)}} V[Q_{\text{IR}}, Q_{\text{R}(i)}]$, for $i = 1, \dots, m$, and $\partial_t^2 Q_{\text{IR}} = -\partial_{Q_{\text{IR}}} V[Q_{\text{IR}}, Q_{\text{R}(i)}]$, which corresponds to a set of $m+1$ coupled differential equations that we solve numerically in the general case. In the absence of coupling with the Raman modes, the IR mode dynamics are described by $\partial_t^2 Q_{\text{IR}} = -\Omega_{\text{IR}}^2 Q_{\text{IR}} - Z^* E_0 \sin(\Omega t) F(t)$. In the resonant case $\Omega = \Omega_{\text{IR}}$, and impulsive limit $\Omega_{\text{IR}} \tau \ll 1$, we find $Q_{\text{IR}}(t) = \sqrt{2\pi} Z^* E_0 \tau / \Omega_{\text{IR}} \cos(\Omega_{\text{IR}} t) \sinh[(\Omega_{\text{IR}} \tau)^2] e^{-(\Omega_{\text{IR}} \tau)^2}$ with boundary conditions $Q_{\text{IR}}(-\infty) = \partial_t Q_{\text{IR}}(-\infty) = 0$ [4].

The amplitude of the excited IR modes scales linearly with the electric field and the mode effective charge.

Now we add coupling with one A_g Raman mode. The potential in Eq. (1) simplifies to $V[Q_{\text{IR}}, Q_{\text{R}}] = \frac{1}{2}\Omega_{\text{IR}}^2 Q_{\text{IR}}^2 + \frac{1}{2}\Omega_{\text{R}}^2 Q_{\text{R}}^2 + \gamma Q_{\text{IR}}^2 Q_{\text{R}}$. The cubic term γ is responsible for the *ionic Raman scattering* [76,78]. Within this mechanism, the infrared active mode is used to drive Raman-scattering processes through anharmonic terms in the potential, and leads to coherent oscillations around a new displaced equilibrium position. Theoretical works have also proposed this cubic nonlinear coupling mechanism to tune magnetic order in RTiO₃ [16,17], investigate light-induced dynamical symmetry breaking [4], modulate the structure of YBa₂Cu₃O and related effects in the magnetic order [18]. On the experimental side, the response of YBa₂Cu₃O_{6+x} to optical pulses has been investigated [79], and experimental detection of possible light-induced superconductivity has been reported [38].

From the equilibrium condition $\partial_{Q_{\text{R}}} V[Q_{\text{IR}}, Q_{\text{R}}] = 0$, we find that the potential is minimized when $Q_{\text{R}} = -\gamma Q_{\text{IR}}^2 / \Omega_{\text{R}}^2$ [7]. Therefore, we obtain larger displaced equilibrium positions effects for low-frequency Raman modes. This argument allows us to limit our discussion to the three low-frequency Raman modes shown in Figs. 2(b)–2(d). Now, considering the cubic term as a perturbation, we find

$$\begin{aligned}
 Q_{\text{R}}(t) &= \frac{\gamma \pi (Z^* E_0 \tau^3)^2 \Omega_{\text{IR}}^2}{(4\Omega_{\text{IR}}^2 - \Omega_{\text{R}}^2) \Omega_{\text{R}}^2} [\Omega_{\text{R}}^2 \cos(2\Omega_{\text{IR}} t) \\
 &+ 2(\Omega_{\text{IR}}^2 - \Omega_{\text{R}}^2) \cos(\Omega_{\text{R}} t) + \Omega_{\text{R}}^2 - 4\Omega_{\text{IR}}^2]. \quad (2)
 \end{aligned}$$

In the resonant limit $\Omega_{\text{R}} = 2\Omega_{\text{IR}}$, the solution is given by $Q_{\text{R}}(t) = -\gamma \pi (Z^* E_0 \tau^3)^2 \sin(\Omega_{\text{IR}} t) [\sin(\Omega_{\text{IR}} t) + \Omega_{\text{IR}} t \cos(\Omega_{\text{IR}} t)] / 2$.

Additional constraints for the IR mode selection arise from current experimental capabilities for strong terahertz pulse generation. Strong fields of up to 100 MV cm⁻¹ have been achieved in the literature in the range 15–50 THz [80,81]. Now we investigate numerically the nonlinear dynamics of the three Raman phonon modes of interest in response to the excitation of a single IR mode. We consider the IR modes with frequencies $\Omega_{\text{IR}} = 6.104$ THz ($Q_{\text{IR}(A)}$) and $\Omega_{\text{IR}} = 6.493$ THz ($Q_{\text{IR}(B)}$), which couple to electric fields parallel to the y and x directions, respectively. The numerical solutions for $Q_{\text{IR}(A)}$ and $Q_{\text{R}(i)}$ are shown in Figs. 3(a) and 3(b) for $E_0 = 4$ MV/cm, and $\tau = 0.2$ ps. $Q_{\text{R}(2)}$ shows the largest amplitude, followed by $Q_{\text{R}(1)}$ which involves displacements in the \hat{z} direction, perpendicular to the layers. $Q_{\text{R}(3)}$ with B_g representation does not participate in the dynamics due to the weak coupling with $Q_{\text{R}(1)}$ and $Q_{\text{R}(2)}$, and the absence coupling with $Q_{\text{IR}(A)}$ at cubic order. In Fig. 3(c) [Fig. 3(d)], we plot the averaged displacements $\langle Q_{\text{R}(i)} \rangle$ as a function of E_0 in response to excitation of $Q_{\text{IR}(A)}$ ($Q_{\text{IR}(B)}$) with $\tau = 0.3$ ps ($\tau = 0.8$ ps). Therefore, the direction of the shift between the layers can be controlled by selectively exciting $\Omega_{\text{IR}(A)}$ or $\Omega_{\text{IR}(B)}$. Next, we will study the magnetic order and show that the induced layer displacements accessible using nonlinear phonon processes can switch the sign of the interlayer exchange interactions.

Effective spin interaction. Recently, theoretical work [82,83] and a combined study employing group theory and ferromagnetic resonance measurements [49] proposed

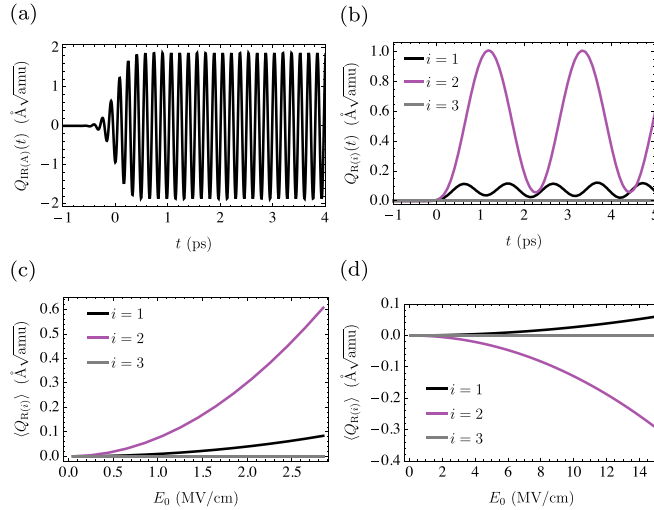


FIG. 3. (a) Infrared $Q_{\text{IR}(A)}$ and (b) Raman modes $Q_{\text{R}(i)}$ oscillations as a function of time for b-CrI₃ for a laser incident in the y direction with $E = 4$ MV/cm, $\tau = 0.2$ ps. (c) [(d)] Average displacement of $Q_{\text{R}(i)}$ nonlinearly coupled to the laser-excited $Q_{\text{IR}(A)}$ ($Q_{\text{IR}(B)}$) with frequency $\Omega_{\text{IR}} = 6.104$ THz ($\Omega_{\text{IR}} = 6.493$ THz). In (c) $\tau = 0.3$ ps and in (d) $\tau = 0.8$ ps.

that CrI₃ is described by the Heisenberg-Kitaev [84,85] Hamiltonian $\mathcal{H} = \mathcal{H}_{\text{intra}} + \mathcal{H}_{\text{inter}}$, where the intralayer Hamiltonian is given by

$$\mathcal{H}_{\text{intra}} = \sum_{(ij) \in \lambda\mu(\nu)} \mathcal{J} \mathbf{s}_i \cdot \mathbf{s}_j + K s_i^\nu s_j^\nu + \Gamma (s_i^\lambda s_j^\mu + s_i^\mu s_j^\lambda),$$

and contains \mathcal{J} Heisenberg and K Kitaev [84] interactions with off-diagonal exchange Γ [85]. The Heisenberg-Kitaev Hamiltonian $\mathcal{H}_{\text{intra}}$ has been studied extensively. For example, the equilibrium phase diagram [85] and the magnon contribution to thermal conductivity has been determined [86], and the spin-wave spectrum has been shown to carry nontrivial Chern numbers [87]. In Ref. [49], the intralayer interaction constants for CrI₃ were determined experimentally to be $\mathcal{J} = -0.2$ meV, $K = -5.2$ meV, and $\Gamma = -67.5$ μeV .

In experiments [48,49], the interlayer Hamiltonian has been assumed to be $\mathcal{H}_{\text{inter}} = \sum_{(ij) \in \text{int.}} J_{\perp} \mathbf{s}_i \cdot \mathbf{s}_j$, with $|J_{\perp}| = 0.03$ meV in Ref. [49], and $|J_{\perp}| = 0.59$ meV in Ref. [48], as extracted from ferromagnetic resonance and inelastic neutron-scattering measurements in bilayer and bulk CrI₃, respectively. Although both experiments propose different intralayer spin models, both find that the interlayer energy scale is much smaller than the intralayer energy scale. Here, we map the interlayer Hamiltonian into a Heisenberg model of the form $\mathcal{H}_{\text{inter}} = \frac{1}{2} \sum_{ij \in \text{int.}} J_{ij} \mathbf{s}_i \cdot \mathbf{s}_j$, and determine J_{ij} from first principles (generalized gradient approximation with Hubbard $U = 1$ eV fixed to reproduce the b-CrI₃ critical temperature $T_C = 45$ K) using a Green's function approach and the magnetic force theorem (for a detailed explanation of the method and applications, see Ref. [88]).

The coupling between the spin and the phonons enters through the interatomic distance dependence of the exchange constants [89]. Under a lattice deformation, and for small deviations from the equilibrium position, the exchange interaction is given by $J[\mathbf{u}(t)] = J^0 + \delta J \hat{\delta} \cdot \mathbf{u}(t) + O[\mathbf{u}(t)^2]$,

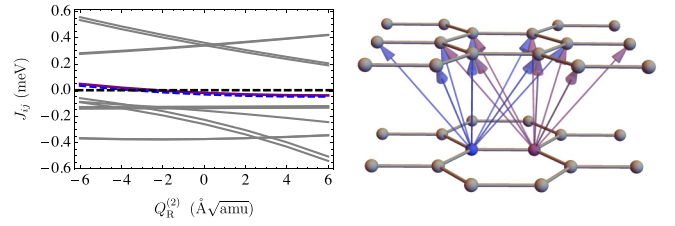


FIG. 4. Left: Interlayer exchange interaction among magnetic moments, up to third-order nearest neighbors, as a function of the Raman displacement $Q_{\text{R}(2)}$. Right: b-CrI₃ sketch, where the arrows indicate the nearest and next-nearest neighbors.

where J^0 corresponds to the equilibrium interaction, δJ is the strength of the first-order correction in the direction $\hat{\delta}$, and $\mathbf{u}(t)$ is the real-space phonon displacement. Given that the infrared phonon frequencies we propose to use ($\Omega_{\text{IR}} \approx 6.49, 6.1$ THz) are much larger than the relevant interlayer interactions ($\lesssim 1$ meV), to leading order, Floquet theory indicates that the effective interlayer exchange interaction becomes $J^{\text{eff}} = J^0 + \delta J \hat{\delta} \cdot \langle \mathbf{u}_{\text{R}} \rangle$, where $\langle \mathbf{u}_{\text{R}} \rangle$ is the time-averaged Raman mode displacement. Therefore, to determine the effect of the nonlinear phonon displacements, we compute the effective exchange interactions in b-CrI₃ for layers displaced with respect to each other in the direction of the low-frequency Raman modes.

The interlayer exchange interactions J_{ij} (up to third-order nearest neighbors) are shown in Fig. 4 as a function of the Raman displacement amplitude $Q_{\text{R}(2)}$, revealing the complexity of the interlayer magnetic order in b-CrI₃. In order to compare our theoretical result for the interlayer interaction with experiments, we define $J_{\perp} \equiv (1/2) \sum_{ij} J_{ij}$. The effective Floquet exchange interaction is then $J_{\perp}^{\text{eff}}(\langle Q_{\text{R}(2)} \rangle) = J_{\perp}^0 + \delta J_{\perp} \langle Q_{\text{R}(2)} \rangle$. We find $J_{\perp}^0 = -0.366$ meV and $\delta J_{\perp} = -0.0713$ meV/($\text{\AA}\sqrt{\text{amu}}$), with $J_{\perp}^{\text{eff}} > 0$, thus preferring FM order, for $\langle Q_{\text{R}(2)} \rangle < -5.13$ $\text{\AA}\sqrt{\text{amu}}$ which corresponds to a real-space displacement of $\sim 3.13\%$ of the Cr-Cr interatomic distance. However, J_{\perp}^0 overestimates the experimental value for b-CrI₃ [49]. Using J_{\perp}^0 as a fitting parameter from experiments, and δJ_{\perp} from our calculations, we find $J_{\perp}^{\text{eff}}(\langle Q_{\text{R}(2)} \rangle) > 0$ for $\langle Q_{\text{R}(2)} \rangle < -0.42$ $\text{\AA}\sqrt{\text{amu}}$, $\sim 0.3\%$ of the Cr-Cr interatomic distance.

Experimentally, $\langle Q_{\text{R}(2)} \rangle \approx 0.5$ $\text{\AA}\sqrt{\text{amu}}$ can be achieved by driving $Q_{\text{IR}(A)}$ with $E_0 = 4$ MV/cm and $\tau = 0.2$ ps. This leads to $Q_{\text{IR}(A)}$ maximum amplitude oscillations ~ 2 $\text{\AA}\sqrt{\text{amu}}$. On the other hand, driving $Q_{\text{IR}(B)}$ with $E_0 = 20$ MV/cm and $\tau = 0.8$ ps, leads to $\langle Q_{\text{R}(2)} \rangle \approx -0.53$ $\text{\AA}\sqrt{\text{amu}}$ with $Q_{\text{IR}(B)}$ reaching maximum amplitude oscillations ~ 1.6 $\text{\AA}\sqrt{\text{amu}}$. Notice that to obtain negative $\langle Q_{\text{R}(2)} \rangle$ displacements, stronger electric fields are required due to the relatively weak coupling of $Q_{\text{IR}(B)}$ with the laser pulse, since the effective charge is $|Z_B^*| = 0.034e/\sqrt{\text{amu}}$, compared to $|Z_A^*| = 0.740583e/\sqrt{\text{amu}}$ for $Q_{\text{IR}(A)}$.

Conclusions. In this work, we studied theoretically b-CrI₃ driven with low-frequency light pulses. We found that coherently driving an infrared mode can activate low-frequency Raman modes involving relative displacements between the layers, which oscillate around new shifted equilibrium positions due to nonlinear phonon processes. These relatively small transient lattice distortions can modify the exchange

interactions and change the sign of the interlayer interaction. This provides the opportunity to change the magnetic order in a system via low-frequency drives. Similar results should be possible for other layered magnetic materials with weak interlayer bonds.

Acknowledgments. We thank Matthias Geilhufe for useful discussions on group theory and the use of GTPack, and D. M. Juraschek for useful discussions on nonlinear phononics. This research was primarily supported by the National Science Foundation through the Center for Dynamics and Control of

Materials: An NSF MRSEC under Cooperative Agreement No. DMR-1720595 and NSF Grant No. DMR-1949701. A.L. acknowledges support from the funding Grant No. PID2019-105488GB-I00. M.R.-V. acknowledges the hospitality of Aspen Center for Physics, supported by National Science Foundation Grant No. PHY-1607611, where parts of this work were performed. M.G.V. acknowledges the Spanish Ministerio de Ciencia e Innovacion (Grant No. PID2019-109905GB-C21) and support from DFG INCIEN2019-000356 from Gipuzkoako Foru Aldundia.

-
- [1] T. Oka and H. Aoki, *Phys. Rev. B* **79**, 081406(R) (2009).
- [2] N. H. Lindner, G. Refael, and V. Galitski, *Nat. Phys.* **7**, 490 (2011).
- [3] M. Först, R. Mankowsky, H. Bromberger, D. Fritz, H. Lemke, D. Zhu, M. Chollet, Y. Tomioka, Y. Tokura, R. Merlin, J. Hill, S. Johnson, and A. Cavalleri, *Solid State Commun.* **169**, 24 (2013).
- [4] A. Subedi, A. Cavalleri, and A. Georges, *Phys. Rev. B* **89**, 220301(R) (2014).
- [5] J. H. Mentink, K. Balzer, and M. Eckstein, *Nat. Commun.* **6**, 6708 (2015).
- [6] M. Gu and J. M. Rondinelli, *Phys. Rev. B* **95**, 024109 (2017).
- [7] D. M. Juraschek, M. Fechner, and N. A. Spaldin, *Phys. Rev. Lett.* **118**, 054101 (2017).
- [8] D. M. Juraschek, M. Fechner, A. V. Balatsky, and N. A. Spaldin, *Phys. Rev. Materials* **1**, 014401 (2017).
- [9] A. Subedi, *Phys. Rev. B* **95**, 134113 (2017).
- [10] M. Babadi, M. Knap, I. Martin, G. Refael, and E. Demler, *Phys. Rev. B* **96**, 014512 (2017).
- [11] J. Liu, K. Hejazi, and L. Balents, *Phys. Rev. Lett.* **121**, 107201 (2018).
- [12] D. M. Juraschek and S. F. Maehrlein, *Phys. Rev. B* **97**, 174302 (2018).
- [13] D. M. Juraschek and N. A. Spaldin, *Phys. Rev. Materials* **3**, 064405 (2019).
- [14] D. M. Juraschek, Q. N. Meier, and P. Narang, *Phys. Rev. Lett.* **124**, 117401 (2020).
- [15] D. M. Juraschek, P. Narang, and N. A. Spaldin, *arXiv:1912.00129*.
- [16] G. Khalsa and N. A. Benedek, *npj Quantum Mater.* **3**, 15 (2018).
- [17] M. Gu and J. M. Rondinelli, *Phys. Rev. B* **98**, 024102 (2018).
- [18] M. Fechner and N. A. Spaldin, *Phys. Rev. B* **94**, 134307 (2016).
- [19] K. Hejazi, J. Liu, and L. Balents, *Phys. Rev. B* **99**, 205111 (2019).
- [20] M. A. Sentef, A. F. Kemper, A. Georges, and C. Kollath, *Phys. Rev. B* **93**, 144506 (2016).
- [21] M. A. Sentef, *Phys. Rev. B* **95**, 205111 (2017).
- [22] N. Tancogne-Dejean, M. A. Sentef, and A. Rubio, *Phys. Rev. Lett.* **121**, 097402 (2018).
- [23] S. Chaudhary, A. Haim, Y. Peng, and G. Refael, *arXiv:1911.07892*.
- [24] S. Chaudhary, D. Hsieh, and G. Refael, *Phys. Rev. B* **100**, 220403(R) (2019).
- [25] M. Vogl, M. Rodriguez-Vega, and G. A. Fiete, *Phys. Rev. B* **101**, 235411 (2020).
- [26] M. Vogl, M. Rodriguez-Vega, and G. A. Fiete, *Phys. Rev. B* **101**, 241408 (2020).
- [27] M. M. Asmar and W.-K. Tse, *arXiv:2003.14383*.
- [28] M. Ke, M. M. Asmar, and W.-K. Tse, *Phys. Rev. Research* **2**, 033228 (2020).
- [29] M. Vogl, P. Laurell, A. D. Barr, and G. A. Fiete, *Phys. Rev. X* **9**, 021037 (2019).
- [30] E. Baldini, C. A. Belvin, M. Rodriguez-Vega, I. O. Ozel, D. Legut, A. Kozłowski, A. M. Oleś, K. Parlinski, P. Piekarczyk, J. Lorenzana, G. A. Fiete, and N. Gedik, *Nat. Phys.* **16**, 541 (2020).
- [31] Z. Gu, H. A. Fertig, D. P. Arovas, and A. Auerbach, *Phys. Rev. Lett.* **107**, 216601 (2011).
- [32] A. Kundu, H. A. Fertig, and B. Seradjeh, *Phys. Rev. Lett.* **116**, 016802 (2016).
- [33] M. Fechner, A. Sukhov, L. Chotorlishvili, C. Kenel, J. Berakdar, and N. A. Spaldin, *Phys. Rev. Materials* **2**, 064401 (2018).
- [34] Y. H. Wang, H. Steinberg, P. Jarillo-Herrero, and N. Gedik, *Science* **342**, 453 (2013).
- [35] F. Mahmood, C.-K. Chan, Z. Alpichshev, D. Gardner, Y. Lee, P. A. Lee, and N. Gedik, *Nat. Phys.* **12**, 306 (2016).
- [36] D. Fausti, R. I. Tobey, N. Dean, S. Kaiser, A. Dienst, M. C. Hoffmann, S. Pyon, T. Takayama, H. Takagi, and A. Cavalleri, *Science* **331**, 189 (2011).
- [37] R. Mankowsky, A. Subedi, M. Först, S. O. Mariager, M. Chollet, H. T. Lemke, J. S. Robinson, J. M. Glowia, M. P. Minitti, A. Frano, M. Fechner, N. A. Spaldin, T. Loew, B. Keimer, A. Georges, and A. Cavalleri, *Nature (London)* **516**, 71 (2014).
- [38] M. Mitranò, A. Cantaluppi, D. Nicoletti, S. Kaiser, A. Perucchi, S. Lupi, P. Di Pietro, D. Pontiroli, M. Riccò, S. R. Clark, D. Jaksch, and A. Cavalleri, *Nature (London)* **530**, 461 (2016).
- [39] J. W. McIver, B. Schulte, F. U. Stein, T. Matsuyama, G. Jotzu, G. Meier, and A. Cavalleri, *Nat. Phys.* **16**, 38 (2020).
- [40] I. Vaskivskiy, J. Gospodaric, S. Brazovskii, D. Svetin, P. Sutar, E. Goresnik, I. A. Mihailovic, T. Mertelj, and D. Mihailovic, *Sci. Adv.* **1**, e1500168 (2015).
- [41] J. Zhang, X. Tan, M. Liu, S. W. Teitelbaum, K. W. Post, F. Jin, K. A. Nelson, D. N. Basov, W. Wu, and R. D. Averitt, *Nat. Mater.* **15**, 956 (2016).
- [42] S. W. Teitelbaum, B. K. Ofori-Okai, Y.-H. Cheng, J. Zhang, F. Jin, W. Wu, R. D. Averitt, and K. A. Nelson, *Phys. Rev. Lett.* **123**, 267201 (2019).
- [43] T. F. Nova, A. S. Disa, M. Fechner, and A. Cavalleri, *Science* **364**, 1075 (2019).
- [44] J. F. Dillon and C. E. Olson, *J. Appl. Phys.* **36**, 1259 (1965).

- [45] M. A. McGuire, H. Dixit, V. R. Cooper, and B. C. Sales, *Chem. Mater.* **27**, 612 (2015).
- [46] N. D. Mermin and H. Wagner, *Phys. Rev. Lett.* **17**, 1133 (1966).
- [47] B. Huang, G. Clark, E. Navarro-Moratalla, D. R. Klein, R. Cheng, K. L. Seyler, D. Zhong, E. Schmidgall, M. A. McGuire, D. H. Cobden, W. Yao, D. Xiao, P. Jarillo-Herrero, and X. Xu, *Nature (London)* **546**, 270 (2017).
- [48] L. Chen, J.-H. Chung, B. Gao, T. Chen, M. B. Stone, A. I. Kolesnikov, Q. Huang, and P. Dai, *Phys. Rev. X* **8**, 041028 (2018).
- [49] I. Lee, F. G. Utermohlen, D. Weber, K. Hwang, C. Zhang, J. van Tol, J. E. Goldberger, N. Trivedi, and P. C. Hammel, *Phys. Rev. Lett.* **124**, 017201 (2020).
- [50] J. L. Lado and J. Fernández-Rossier, *2D Mater.* **4**, 035002 (2017).
- [51] Z. Wang, I. Gutiérrez-Lezama, N. Ubrig, M. Kroner, M. Gibertini, T. Taniguchi, K. Watanabe, A. Imamoğlu, E. Giannini, and A. F. Morpurgo, *Nat. Commun.* **9**, 2516 (2018).
- [52] T. Song, X. Cai, M. W.-Y. Tu, X. Zhang, B. Huang, N. P. Wilson, K. L. Seyler, L. Zhu, T. Taniguchi, K. Watanabe, M. A. McGuire, D. H. Cobden, D. Xiao, W. Yao, and X. Xu, *Science* **360**, 1214 (2018).
- [53] K. L. Seyler, D. Zhong, D. R. Klein, S. Gao, X. Zhang, B. Huang, E. Navarro-Moratalla, L. Yang, D. H. Cobden, M. A. McGuire, W. Yao, D. Xiao, P. Jarillo-Herrero, and X. Xu, *Nat. Phys.* **14**, 277 (2018).
- [54] D. R. Klein, D. MacNeill, J. L. Lado, D. Soriano, E. Navarro-Moratalla, K. Watanabe, T. Taniguchi, S. Manni, P. Canfield, J. Fernández-Rossier, and P. Jarillo-Herrero, *Science* **360**, 1218 (2018).
- [55] Z. Sun, Y. Yi, T. Song, G. Clark, B. Huang, Y. Shan, S. Wu, D. Huang, C. Gao, Z. Chen, M. McGuire, T. Cao, D. Xiao, W.-T. Liu, W. Yao, X. Xu, and S. Wu, *Nature (London)* **572**, 497 (2019).
- [56] L. Thiel, Z. Wang, M. A. Tschudin, D. Rohner, I. Gutiérrez-Lezama, N. Ubrig, M. Gibertini, E. Giannini, A. F. Morpurgo, and P. Maletinsky, *Science* **364**, 973 (2019).
- [57] N. Ubrig, Z. Wang, J. Teyssier, T. Taniguchi, K. Watanabe, E. Giannini, A. F. Morpurgo, and M. Gibertini, *2D Mater.* **7**, 015007 (2020).
- [58] B. Huang, G. Clark, D. R. Klein, D. MacNeill, E. Navarro-Moratalla, K. L. Seyler, N. Wilson, M. A. McGuire, D. H. Cobden, D. Xiao, W. Yao, P. Jarillo-Herrero, and X. Xu, *Nat. Nanotechnol.* **13**, 544 (2018).
- [59] T. Song, Z. Fei, M. Yankowitz, Z. Lin, Q. Jiang, K. Hwangbo, Q. Zhang, B. Sun, T. Taniguchi, K. Watanabe, M. A. McGuire, D. Graf, T. Cao, J.-H. Chu, D. H. Cobden, C. R. Dean, D. Xiao, and X. Xu, *Nat. Mater.* **18**, 1298 (2019).
- [60] N. Sivadas, S. Okamoto, X. Xu, C. J. Fennie, and D. Xiao, *Nano Lett.* **18**, 7658 (2018).
- [61] S. W. Jang, M. Y. Jeong, H. Yoon, S. Ryee, and M. J. Han, *Phys. Rev. Materials* **3**, 031001 (2019).
- [62] D. Soriano, C. Cardoso, and J. Fernandez-Rossier, *Solid State Commun.* **299**, 113662 (2019).
- [63] D. Soriano and M. I. Katsnelson, *Phys. Rev. B* **101**, 041402(R) (2020).
- [64] K. Momma and F. Izumi, *J. Appl. Crystallogr.* **44**, 1272 (2011).
- [65] P. Jiang, C. Wang, D. Chen, Z. Zhong, Z. Yuan, Z.-Y. Lu, and W. Ji, *Phys. Rev. B* **99**, 144401 (2019).
- [66] See Supplemental Material at <http://link.aps.org/supplemental/10.1103/PhysRevB.102.081117> for full details of the first-principles calculations for phonon frequencies, non-linear coefficients, and exchange interactions and further group theory aspects, which includes the additional references [90–92].
- [67] E. Kroumova, M. Aroyo, J. Perez-Mato, A. Kirov, C. Capillas, S. Ivantchev, and H. Wondratschek, *Phase Transitions* **76**, 155 (2003).
- [68] M. S. Dresselhaus, G. Dresselhaus, and A. Jorio, *Group theory: Application to the Physics of Condensed Matter* (Springer-Verlag, Berlin/Heidelberg, 2008).
- [69] R. M. Geilhufe and W. Hergert, *Front. Phys.* **6**, 86 (2018).
- [70] W. Hergert and M. R. Geilhufe, *Group theory in Solid State Physics and Photonics: Problem Solving with Mathematica* (Wiley-VCH, Weinheim, 2018).
- [71] P. Giannozzi *et al.*, *J. Phys.: Condens. Matter* **21**, 395502 (2009).
- [72] P. Giannozzi *et al.*, *J. Phys.: Condens. Matter* **29**, 465901 (2017).
- [73] G. Kresse and J. Furthmüller, *Comput. Mater. Sci.* **6**, 15 (1996).
- [74] G. Kresse and J. Furthmüller, *Phys. Rev. B* **54**, 11169 (1996).
- [75] S. Baroni, S. de Gironcoli, A. Dal Corso, and P. Giannozzi, *Rev. Mod. Phys.* **73**, 515 (2001).
- [76] M. Först, C. Manzoni, S. Kaiser, Y. Tomioka, Y. Tokura, R. Merlin, and A. Cavalleri, *Nat. Phys.* **7**, 854 (2011).
- [77] X. Gonze and C. Lee, *Phys. Rev. B* **55**, 10355 (1997).
- [78] R. F. Wallis and A. A. Maradudin, *Phys. Rev. B* **3**, 2063 (1971).
- [79] R. Mankowsky, M. Först, T. Loew, J. Porras, B. Keimer, and A. Cavalleri, *Phys. Rev. B* **91**, 094308 (2015).
- [80] A. Sell, A. Leitenstorfer, and R. Huber, *Opt. Lett.* **33**, 2767 (2008).
- [81] T. Kampfrath, K. Tanaka, and K. A. Nelson, *Nat. Photonics* **7**, 680 (2013).
- [82] C. Xu, J. Feng, H. Xiang, and L. Bellaiche, *npj Comput. Mater.* **4**, 57 (2018).
- [83] C. Xu, J. Feng, M. Kawamura, Y. Yamaji, Y. Nahas, S. Prokhorenko, Y. Qi, H. Xiang, and L. Bellaiche, *Phys. Rev. Lett.* **124**, 087205 (2020).
- [84] A. Kitaev, *Ann. Phys.* **321**, 2 (2006).
- [85] J. G. Rau, Eric Kin-Ho Lee, and H.-Y. Kee, *Phys. Rev. Lett.* **112**, 077204 (2014).
- [86] G. L. Stamokostas, P. E. Lapas, and G. A. Fiete, *Phys. Rev. B* **95**, 064410 (2017).
- [87] P. A. McClarty, X.-Y. Dong, M. Gohlke, J. G. Rau, F. Pollmann, R. Moessner, and K. Penc, *Phys. Rev. B* **98**, 060404(R) (2018).
- [88] M. Hoffmann, A. Ernst, W. Hergert, V. N. Antonov, W. A. Adeagbo, R. Matthias Geilhufe, and H. Ben Hamed, *Phys. Status Solidi B* **257**, 1900671 (2020).
- [89] E. Granado, A. García, J. A. Sanjurjo, C. Rettori, I. Torriani, F. Prado, R. D. Sánchez, A. Caneiro, and S. B. Oseroff, *Phys. Rev. B* **60**, 11879 (1999).
- [90] H. T. Stokes, D. M. Hatch, and B. J. Campbell, “Isodistort, Isotropy Software Suite, iso.byu.edu”.
- [91] D. T. Larson and E. Kaxiras, *Phys. Rev. B* **98**, 085406 (2018).
- [92] S. Djurdjic Mijin, A. Šolajić, J. Pešić, M. Šćepanović, Y. Liu, A. Baum, C. Petrovic, N. Lazarević, and Z. V. Popović, *Phys. Rev. B* **98**, 104307 (2018).